THE JOURNAL OF PHYSICAL CHEMISTRY A
A JOURNAL OF THE AMERICAN CHEMICAL SOCIETY

pubs.acs.org/JPCA Article

Equatorial Ligation Controls 5f Electron Binding in Penta- and Hexavalent Uranyl Acetate Complexes

Burak A. Tufekci,[§] Taylor Gregory,[§] Shiying Wang, Kathryn Foreman, Tatsuya Chiba, Evangelos Miliordos,* and Kit H. Bowen*

Cite This: J. Phys. Chem. A 2026, 130, 1829−1836 Read Online

ACCESS | Metrics & More | Article Recommendations | Supporting Information

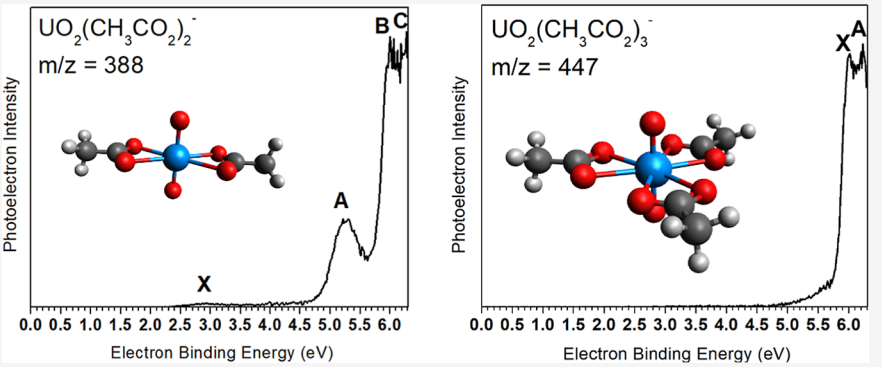

ABSTRACT: Anion photoelectron spectroscopy (aPES), in conjunction with relativistic electronic-structure calculations, probed the electronic structures of the di- and triacetate uranyl complex anions, $(AcO)_2UO_2^-$ and $(AcO)_3UO_2^-$. These anions were generated by electrospray and photodetached at 355 nm for the diacetate and 193 nm for both species. The experimentally assigned vertical electron detachment energies are 2.77 and 6.02 eV for the di- and triacetate complexes, respectively. Electronic-structure calculations were performed to reproduce the aPES spectra. Wave function analysis indicates a $U^V(5f^1)$ center for $(AcO)_2UO_2^-$ and a $U^{VI}(5f^0)$ center for $(AcO)_3UO_2^-$. Therefore, the detached electron is the $5f^1$ electron of the former, which leads to significant spin−orbit effects, while for the latter, the detached electron comes from an acetate oxygen. In both systems, all U−O bonds are highly ionic with minimal covalent character. Our experimental measurements in tandem with our computational findings highlight how higher coordination numbers can adjust the degree of 5f electron participation in bonding and increase the stabilization of the anion.

1. INTRODUCTION

Understanding how organic ligands coordinate with uranyl in aqueous environments is central to nuclear-waste management and environmental remediation.[1−4] The most stable form of uranium, uranyl ion (UO_2^{2+}), is already prevalent in soils as byproducts of uranium mining and liquid nuclear waste.[5,6] Beyond waste management, uranyl complexation has been explored as a pathway toward isotope separation. Conventional enrichment methods such as centrifugation, gaseous diffusion, laser isotope separation, and aerodynamic methods[7−9] require volatile uranium compounds.[10] In contrast, chemical-exchange and ion-exchange methods exploit subtle differences in the physicochemical behavior of uranium isotopes between different oxidation states.[7−15] In uranyl−ligand systems, chromatographic studies have demonstrated reversible isotope effects in ligand-exchange reactions on both cation- and anion-exchange resins.[16−19] With regards to isotope separation, ^{235}U has been shown to accumulate preferentially in uranyl acetate complexes during isotopic exchange reactions with the aquauranyl ion.[17] In addition, carboxylates such as acetate govern actinide complexation in humic-rich soils, and studying how they interact with the uranyl ion is essential for understanding the mobility and mitigation of uranium in natural ecosystems.[20,21] Infrared (IR) spectroscopy indicates that carboxylate ligands (e.g., acetate, citrate, and lactate) weaken the UO bond in uranyl, shifting the asymmetric OUO stretching mode (ν_3) to lower frequencies. By varying the ligands coordinated to uranyl, an empirical relationship between ν_3 and the isotope-separation coefficient ϵ was determined.[22−26]

Currently, mitigation strategies are aimed at controlling uranium solubility and mobility via ligand complexation, which

Received: January 8, 2026
Revised: February 5, 2026
Accepted: February 6, 2026
Published: February 18, 2026

often rely on redox reactions that control uranium solubility in groundwater systems. U(VI) species are readily soluble in oxidizing environments, whereas U(IV) precipitates in anaerobic, reducing environments.[13−15,27−30] While pentavalent uranyl U(V) is stable in concentrated carbonate solution, it undergoes disproportionation to U(IV) and U(VI) and is unstable in aqueous solutions.[11,12,31] Aside from its fundamental interest, pentavalent uranyl ($U^{V}O_2^{+}$) is a key intermediate in redox chemistry such as photocatalysis[32] as well as bacterial and mineral reduction of soluble hexavalent uranyl species to insoluble U(IV).[33−36] Despite the synthetic challenges associated with pentavalent uranyl, there is considerable interest in isolating it and elucidating its electronic structure. Recently, monomeric and dimeric uranyl(V) amide complexes were synthesized, enabling the assignment of the quartet dominated excited state of $U^{V}O_2^{+}$ through emission and Raman spectroscopy.[37]

From an electronic-structure perspective, the chemical bonding in hexavalent uranyl UO_2^{2+} is often described in terms of two U−O triple bonds, each formed between uranium and an oxo ligand. These bonds are facilitated by mixing between the uranium 5f and 6d orbitals and the oxygen 2p orbitals.[38] The uranium 7s orbital does not participate in bonding; however, the lowest-lying virtual molecular orbitals $5f\delta_u$, $5f\varphi_u$, and $6d\delta_g$ remain available to interact with σ- and π-donor equatorial ligands.[39−41] UO_2^{2+} can possess coordination numbers ranging from 4 to 6 in the equatorial plane and can readily accommodate 5 or 6 equatorial donor ligands in pentagonal or hexagonal bipyramidal geometries.[39,41−44] However, little is known about the chemical behavior and electronic structure of pentavalent uranyl (UO_2^{+}). In a phenomenon known as cation−cation interaction (CCI), the UO_2^{+} can coordinate with other cations via their electron-donor O atoms in an "extreme dipole interaction".[45−47] Regardless, the U(V) system contains an essentially isolated $5f^1$ electron, making it an ideal probe for studying the chemical behavior of 5f electrons spectroscopically.[48,49]

In terms of practicality, available organic oxygen-donor ligands are attractive tools for exploring new facets of uranyl chemistry. Acetate is an electron-rich, oxygen-donor Lewis base that coordinates Lewis-acidic metal centers, such as uranyl, by donating their lone pairs. Acetate, abundant in groundwater and soils, is a simple carboxylate bioligand that can bind monodentate or bidentate to electron-deficient centers.[50] Infrared multiple photon dissociation (IRMPD) combined with density functional theory (DFT) demonstrated that gas-phase uranyl triacetate anions, although capable of forming a fully bidentate structure, predominately adopt a mixed-denticity arrangement with two bidentate acetates and one monodentate acetate.[51] Owing to this variable denticity, acetate is a potential model ligand for probing uranyl coordination chemistry.[52−54]

Here, we are interested in elucidating the electronic structure of two uranyl acetate complexes $(AcO)_2UO_2^{-}$ and $(AcO)_3UO_2^{-}$ with formally U(V) and U(VI) oxidation states, respectively. Gas-phase studies combined with high-level quantum chemical calculations provide the ideal setting for this purpose. We used anion photoelectron spectroscopy (aPES) of mass-selected, ligated uranyl acetate anions generated by electrospray ionization (ESI) and interpreted their respective spectra with high-level electronic-structure calculations. ESI has proven successful at producing ligated uranyl complexes in the gas phase,[51,54−59] but to our knowledge, no ligated uranyl complex anions have yet been photodetached to yield aPES spectra.[34,41−46] Our findings reveal how increasing acetate coordination tunes the electronic structure of the uranyl center and affects the electron affinity of the system, which changes substantially from 2.63 to 6.02 eV.[60,61]

2. METHODS

2.1. Experimental Methods

Uranyl acetate anions were prepared by reacting uranium tetrachloride, UCl_4 (United Nuclear), with ammonium acetate (NH_4^{+} AcO^{-}) in a 3:1 molar ratio in dry acetonitrile. This reaction produced a water-soluble solid precipitate and most likely ammonium chloride ($NH_4^{+}Cl^{-}$). Ions from this solution were extracted into the gas phase from solution using a home-built electrospray ionization (ESI) apparatus, described in detail in a previous publication.[62] Briefly, the solution was continuously sprayed through a fused silica capillary floated at −1.5−2 kV into a series of ion optical lenses as well as quadrupole and octupole ion guides into a Paul ion trap where the anions were translationally cooled via collisions with a buffer gas composed of 20% H_2 in He that thermalizes the anions to room temperature (300 K). Increasing the ion trap voltage allowed for trapping of heavier anions. The anions were then released from the trap in synchronization with the Wiley−McLaren time-of-flight mass spectrometer (TOFMS), which has been previously described in detail.[63] The resulting mass spectra are shown in Figure 1.

aPES was conducted by crossing a mass-selected and momentum-decelerated packet of the anions of interest with photons of varying energies ($h\nu$) from two fixed-frequency lasers: a Nd:YAG laser (355 nm) and an ArF excimer laser (193 nm). The resulting electron

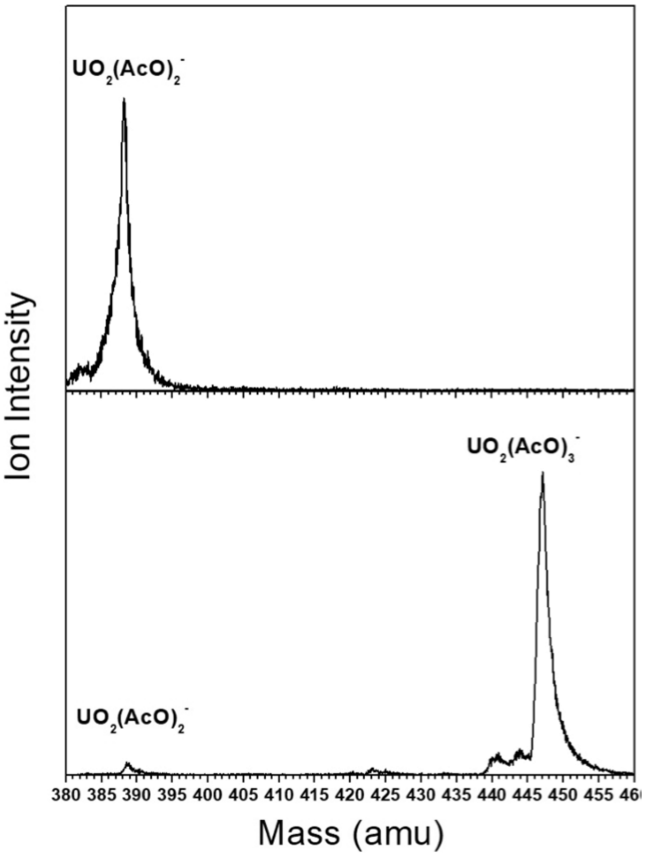

Figure 1. Mass spectra from ESI of a dry acetonitrile reaction solution mixture of UCl_4 and NH_4AcO (1:3). Tuning the ion trap RF voltage preferentially filtered the high-mass triacetate complex.

https://doi.org/10.1021/acs.jpca.6c00067
J. Phys. Chem. A 2026, 130, 1829−1836

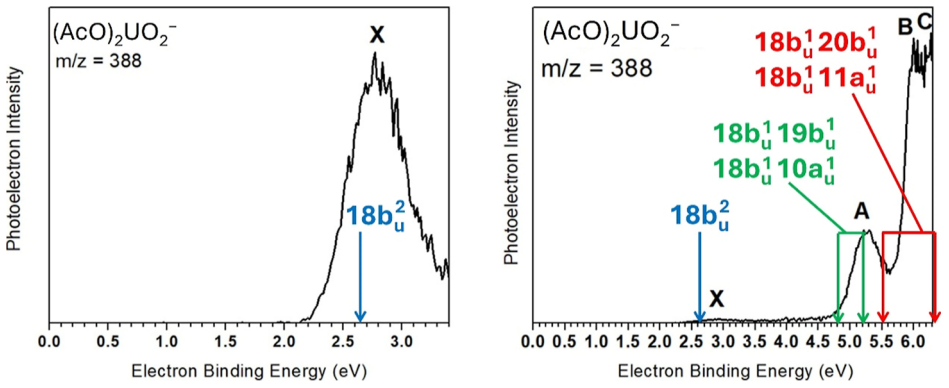

Figure 2. Photoelectron spectra of $(AcO)_2UO_2^-$ at 300 K: the 355 nm (3.49 eV) spectrum is shown on the left and the 193 nm (6.42 eV) spectrum on the right. Theoretically predicted peak positions and electronic configurations of the lowest-energy states of $(AcO)_2UO_2^-$ are shown with arrows; connected arrows indicate multiple electronic states in that region.

kinetic energies (EKEs) from the photodetached anions were measured using a magnetic bottle photoelectron spectrometer, with a resolution of approximately 50 meV at 1 eV EKE. The electron binding energy (EBE) was calculated using the relation $h\nu$ = EKE + EBE, where $h\nu$ is the energy of the photons used for photodetachment. The photoelectron spectra were calibrated with the known electron affinity and atomic transitions of iodine.

2.2. Computational Details

Electronic-structure calculations were performed on gas-phase uranyl acetate complexes with two or three acetate ligands in their neutral and anionic charge states. As expected, both scalar relativistic and spin−orbit effects are necessary for accurate calculations of UO_2^{2+}-containing compounds.[64] We first optimized the geometries of the anionic species at the DFT level of theory using the B3LYP density functional combined with triple-ζ quality basis sets. The Cartesian coordinates of the optimized geometries are given in Table S1 of the Supporting Information (SI). The plain cc-pVTZ set was used for C and H centers,[65] while oxygen atoms were equipped with a series of diffuse functions (aug-cc-pVTZ)[66] to account for their anionic character. For U, we employed the cc-pVTZ-PP basis set combined with the appropriate relativistic pseudopotential.[67,68] The Cartesian coordinates of the optimized structures are given in Table S1. For these calculations, we invoked the Gaussian 16 suite of codes.[69]

For $(AcO)_2UO_2^-$, vertical electron detachment energies (VEDEs) were obtained from single-point CCSD(T) and MRCI + Q calculations at the DFT-optimized anion geometries using the following expression:

$$\mathrm{VEDE} = \mathrm{VEDE(X;CCSD(T))} + \Delta\mathrm{E(MRCI + Q/SO)} + \mathrm{SO(X^-;\ MRCI + Q/SO)}$$

where VEDE(X; CCSD(T)) is the energy difference between the ground states of the anionic and neutral species, ΔE(MRCI + Q/SO) are the excitation energies at the MRCI + Q (MRCI + Davidson correction) level and correcting for spin−orbit effects, and SO(X^-; MRCI + Q/SO) is the spin−orbit correction for the ground state of the anion. The spin−orbit calculations were carried out by diagonalizing the Breit−Pauli Hamiltonian in the MRCI space but replacing the MRCI energies (diagonal elements) with the corresponding MRCI + Q energies. The reference CASSCF wave functions were constructed with an active space of 5 orbitals (see Figure 3) containing 2 electrons (neutral) or 3 electrons (anions). For the MRCI and CCSD(T) calculations, we exploited the symmetry elements of C_{2h}. All valence electrons are correlated at the CCSD(T) level, while we used the smallest core space that was technically possible for MRCI (28 core orbitals). For $(AcO)_3UO_2^-$ and for reasons that will be provided in the discussion below, the VEDE values were calculated at the MP2 level of theory correlating all valence electrons. All multireference, MP2, and CCSD(T) calculations were done with Molpro2021.3.[70]

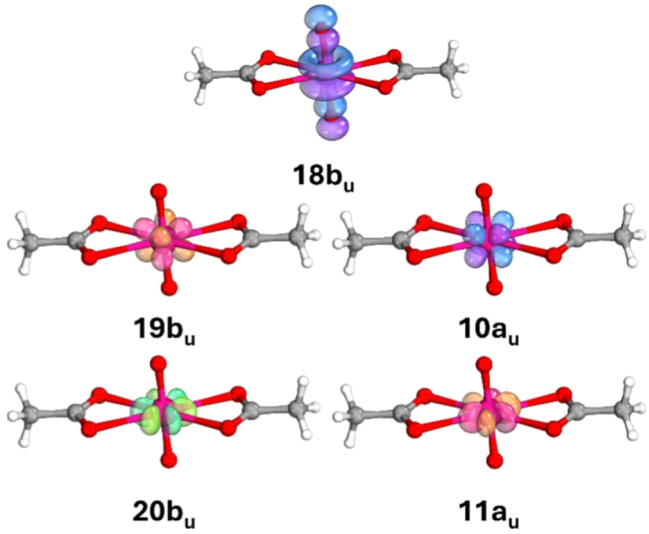

Figure 3. Contours of select molecular orbitals of $(AcO)_2UO_2^-$ relevant to the lowest energy states.

3. RESULTS AND DISCUSSION

3.1. aPES of $(AcO)_2UO_2^-$

Figure 2 displays the recorded photoelectron spectra of $UO_2(AcO)_2^-$ along with our predicted positions for peaks corresponding to the excited states discussed earlier. The vertical detachment energy (VDE), which according to the Franck−Condon principle corresponds to the maximum overlap between the anionic and neutral vibrational wave function, appears as peak X, at 2.77 eV. Higher electron binding energy (EBE) values occur at 5.27 eV (peak A) as well as a pair of peaks at 6.01 and 6.28 eV, labeled as peaks B and C, respectively. The small peak at around 2.5−3.0 eV correlates very well with our calculated VEDE value of 2.63 eV = 2.26 eV [VEDE(X; CCSD(T))] + 0.37 eV [SO(X^-; MRCI + Q/SO)], while the strong peaks at 5.0−5.5 eV and 5.6−6.3 eV match well with our multiple spin−orbit states in the ranges of 4.8−5.2 eV and 5.5−6.4 eV (see Table S3 of the SI).

The ground state of $(AcO)_2UO_2^-$ is a doublet state with one unpaired electron populating one of the two 5fδ_u orbitals of U (see $10a_u$ of Figure 3). Three other electronic states lie within 0.9 eV from the ground state, populating the $19b_u$ (5fδ_u), $11a_u$ (5fφ_u), and $20b_u$ (5fφ_u) orbitals of Figure 3. The spin−orbit wave functions demonstrate extensive mixing of these four

https://doi.org/10.1021/acs.jpca.6c00067
J. Phys. Chem. A 2026, 130, 1829−1836

electronic states. The excitation energies and composition of these wave functions are listed in Table S2 of the SI. Removing the $10a_u$ electron leads to the closed-shell ground state of $(AcO)_2UO_2$, while the lowest-lying excited electronic states of $(AcO)_2UO_2$ are formed by promoting one electron from the doubly occupied $18b_u$ orbital (see Figure 3) to one of the $10a_u$, $11a_u$, $19b_u$, or $20b_u$ orbitals. All five involved orbitals are localized on uranium and only $18b_u$ is a combination of the $5f_z^3$ of uranium and the $2p_z$ orbitals of the uranyl oxygen atoms. All our VEDE values and composition of the wave functions after spin−orbit corrections are listed in Table S3 of the SI. The position of the theoretically predicted peaks is shown as arrows in Figure 2 and is consistently placed in lower energies (by 0.2−0.3 eV) than the experimental peaks.

3.2. aPES of $(AcO)_3UO_2^-$

The $(AcO)_3UO_2^-$ species is a highly stable anion with a closed-shell singlet ground state. The aPES spectrum in Figure 4 suggests an experimental VDE value of 6.02 eV (peak X) and

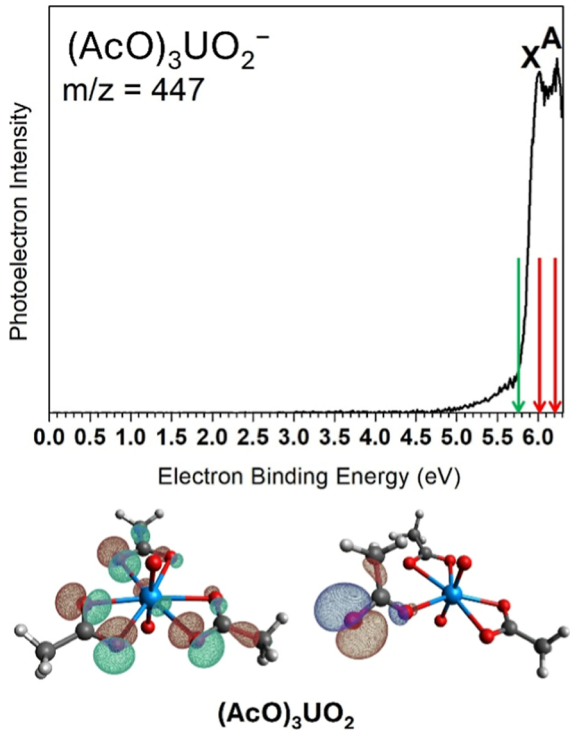

Figure 4. Photoelectron spectra of $(AcO)_3UO_2^-$ at 300 K and 193 nm (6.42 eV) along with the computationally predicted positions (green and red arrows for the ground and excited states). The singly occupied orbital of the neutral $(AcO)_3UO_2$ species at its optimized geometry and the optimized geometry of the anion are shown in the bottom right and left contours, respectively.

an adiabatic electron affinity (AEA) larger than 4.5 eV (end of the tail of the band onset of X). The optimal structure of $(AcO)_3UO_2^-$ bears three acetate ligands on the plane perpendicular to the UO_2^{2+} unit (see Figure 4).[52] Compared to $(AcO)_2UO_2^-$, which contains a UO_2^+ unit, there is no unpaired electron to be ejected, and thus, ionization occurs from the oxygen atoms of the acetate ligands. The ground state of $(AcO)_3UO_2$ is formed by removing one electron from a σ_{UO} orbital (ionic $U^{5+}\cdots AcO^-$ interaction; see Figure 4), which leads to the disruption of one U−AcO bond (see the optimized structure of Figure 4 and Table S1 of the SI for Cartesian coordinates).

Using the optimized geometry of the $(AcO)_3UO_2$, we were able to locate a new structure (local minimum = LM) for $(AcO)_3UO_2^-$ resembling that of $(AcO)_3UO_2$ (see coordinates in Table S1 of the SI), which is 0.22 eV higher than the global minimum (GM) symmetric structure separated by a transition with a GM → LM energy barrier of 0.35 eV, and thus, LM is not expected to be present under the experimental conditions. Due to the size of the system, we were unable to perform CCSD or CCSD(T) calculations. Also, spin−orbit effects are expected to be marginal here since only the 2p orbitals of oxygen atoms are involved. We thus decided to perform MP2 calculations, which showed consistent results with the experimental findings. Using the GM structure, our MP2 VEDE value is 5.72 eV compared well with the experimental value for the X peak at 6.02 eV. Removal of electrons from other σ or π orbitals of acetate oxygen atoms provides VEDE values (6.01, 6.16, 6.37, and 6.44 eV) that can account for peak A at 6.3 eV. Using the LM structure, our MP2VEDE is 5.50 eV, while the MP2 AEA value is 5.20 eV. Conclusively, the very different structures of $(AcO)_3UO_2^-$ and $(AcO)_3UO_2$ can rationalize the presence of the tail in our aPES spectrum in the 4.5−5.8 eV region.

Our observations are in harmony with the aPES study of Wang and Li on similar systems with composition $X_3UO_2^-$, where X = F, Cl, Br, and I.[38] Apart from X = F, all other systems lose one of their valence p-orbitals (3p, 4p, or 5p). The measured VEDE values, 6.72, 6.37, and 5.72 eV, for X = Cl, Br, and I, respectively, correlate linearly with the VEDE values of the corresponding plain anions (X^-) of 3.61, 3.36, and 3.06 eV,[71] and they are on average 83% larger (probably due to the $U^{6+}\cdots X^-$ interaction). Applying this correlation to X = AcO, we find a VEDE value for $(AcO)_3UO_2^-$ equal to 1.8 × 3.25 eV[72] = 5.95 eV, which is close to our observed 6.02 eV. Also, for X = Cl, Br, and I, there are multiple excited states of X_3UO_2 within 0.5 eV corresponding to the removal of different valence p-electrons of X.[38]

3.3. Chemical Bonding Considerations

The central UO_2 unit of the two employed species appears as UO_2^+ and UO_2^{2+} in $(AcO)_2UO_2^-$ and $(AcO)_3UO_2^-$, respectively. The ground state of the latter is a closed-shell species, and the first excited states are produced by promoting one electron from the σ_u orbital (resembling $18b_u$ of Figure 3) to one of the δ_u or φ_u (resembling $19b_u/10a_u$ $20b_u/11a_u$ of Figure 3) orbitals, all of them being mainly localized on uranium.[73,74] While the electronic structure of UO_2^+ has been investigated in prior gas-phase spectroscopic[75] and quantum chemical calculations,[76] including the identification of a $5f^1$ ground-state configuration, its behavior in ligated complexes remains considerably underexplored. The ground state of UO_2^+ can be created by adding one δ_u or φ_u electron to UO_2^{2+} and its excited states stem from the promotion to other δ_u or φ_u orbitals. Spin−orbit effects cause considerable mixing of all these four configurations (see Table S2 of the SI). Ligated UO_2^+ species have been observed in solutions by photoexciting the corresponding UO_2^{2+} species, which oxidize one ligand or solvent molecule to produce UO_2^+ centers.[77] Similarly, here, we produce the UO_2^+ and UO_2^{2+} species by controlling the coordination number with acetate ligands.

Another aspect for f-block metal complexes is the extent to which 5f- or 6d-orbitals participate in bonding.[78] The occupied

https://doi.org/10.1021/acs.jpca.6c00067
J. Phys. Chem. A 2026, 130, 1829−1836

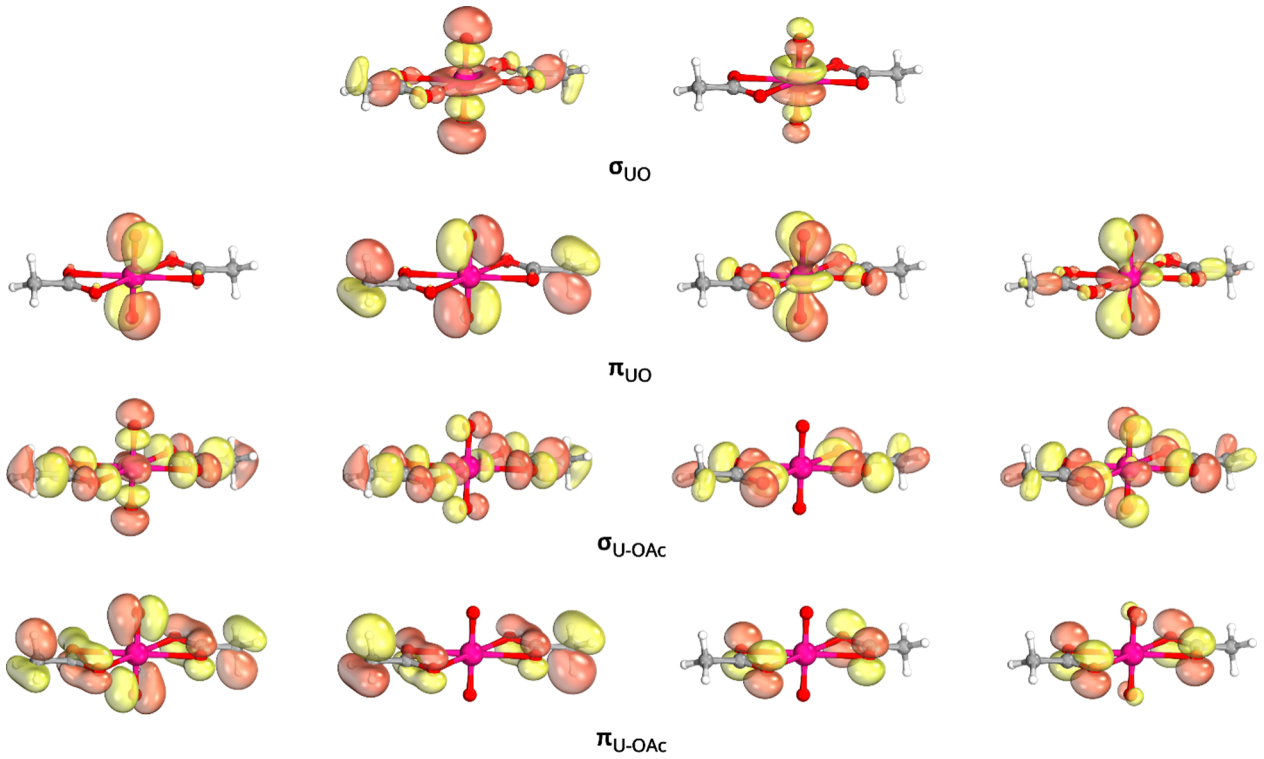

Figure 5. Select bonding molecular orbitals of $(AcO)_2UO_2^-$ relevant to the chemical bonding between uranium and oxygen or acetate ligands.

molecular orbitals for $(AcO)_2UO_2^-$ collected in Figure 5 indicate two groups, one corresponding to the UO_2 unit and one to the acetate ligands suggesting primarily ionic bonds between the acetate ligands and U^{5+}. The bonding in UO_2^{2+} is represented by the σ_{UO} and π_{UO} orbitals of Figure 5. The σ_{UO} orbitals can be clearly seen as the symmetric and antisymmetric combination of the two σ_{UO} bonds, which are facilitated by the $6d_{z^2}$ and $5f_{z^3}$ of uranium and are polarized toward oxygen and uranium, respectively. Similarly, for symmetry reasons, two of the four π_{UO} bonding orbitals can be facilitated by the $6d_{xz}$ and $6d_{yz}$ ($6d_{\pm1}$) uranium orbitals, while the other two by the $5f_{xz^2}$ and $5f_{yz^2}$ ($5f_{\pm1}$) orbitals. Again, the former are clearly polarized toward oxygen, and the latter have major $5f_{\pm1}$ contribution. Based on these observations, the O≡U≡O picture can be supported, but the bonding orbitals indicate polarized UO bonds pointing to a considerable ionic $O^{2-}U^{6+}O^{2-}$ character. The σ and π orbitals pertaining to the acetate ligands are rather localized and show small mixing with uranium orbitals suggesting primarily ionic interactions.

4. CONCLUSIONS

In this work, we combined aPES with high-level electronic-structure calculations to elucidate how acetate ligation modulates the electronic structure of uranyl and the role of 5f electrons in electron detachment in its di- and triacetate forms. By directly comparing pentavalent and hexavalent uranyl acetate complexes, our results illustrate how changes in valence electron configuration can modulate 5f participation in bonding. These results demonstrate that increasing equatorial coordination not only stabilizes the anions but also fundamentally alters the character of the electron being detached, shifting from a 5f-derived electron in the diacetate to an acetate-based electron in the triacetate. These findings highlight how the coordination number governs the extent of 5f involvement in bonding and, more broadly, how simple carboxylate ligands can modulate the uranyl electronic structure. This work establishes acetate as an effective model ligand for probing uranyl–ligand interactions in the gas phase and a foundation for future gas-phase studies on ligated uranyl complexes displaying various degrees of valency.

■ ASSOCIATED CONTENT

Supporting Information

The Supporting Information is available free of charge at https://pubs.acs.org/doi/10.1021/acs.jpca.6c00067.

Cartesian coordinates for all B3LYP-optimized structures and detailed electronic-structure data, including excitation energies, VEDEs, and wave function compositions at the MRCI + Q/SO level (PDF)

■ AUTHOR INFORMATION

Corresponding Authors

Evangelos Miliordos − *Department of Chemistry, Auburn University, Auburn, Alabama 36849, United States;* orcid.org/0000-0003-3471-7133; Email: emiliord@auburn.edu

Kit H. Bowen − *Department of Chemistry, Johns Hopkins University, Baltimore, Maryland 21218, United States;* orcid.org/0000-0002-2858-6352; Email: kbowen@jhu.edu

Authors

Burak A. Tufekci − *Department of Chemistry, Johns Hopkins University, Baltimore, Maryland 21218, United States;* orcid.org/0000-0002-6964-6630

https://doi.org/10.1021/acs.jpca.6c00067
J. Phys. Chem. A 2026, 130, 1829−1836

Taylor Gregory − *Department of Chemistry, Auburn University, Auburn, Alabama 36849, United States;* orcid.org/0009-0005-4990-7409
Shiying Wang − *Department of Chemistry, Johns Hopkins University, Baltimore, Maryland 21218, United States;* orcid.org/0009-0007-6318-8580
Kathryn Foreman − *Department of Chemistry, Johns Hopkins University, Baltimore, Maryland 21218, United States;* orcid.org/0000-0002-7388-8165
Tatsuya Chiba − *Department of Chemistry, Johns Hopkins University, Baltimore, Maryland 21218, United States;* orcid.org/0000-0002-9189-1309

Complete contact information is available at: https://pubs.acs.org/10.1021/acs.jpca.6c00067

Author Contributions

§B.A.T and T.G. contributed equally to this work. B.A.T, S.Y.W, K.F., and T.C. completed the experimental work and T.G. and E.M. completed the computational work. K.H.B. conceived of and supervised the work.

Notes

The authors declare no competing financial interest.

■ ACKNOWLEDGMENTS

The experimental material in this work was supported by the Heavy Elements Chemistry (HEC) program of the Department of Energy (DOE) under grant number DE-SC0022977 (K.H.B.). E.M. and T.G. are indebted to Auburn University (AU) for financial support. E.M. is especially grateful to the donors of the James E. Land endowment. This work was completed using resources provided by the Auburn University Easley Cluster.

■ REFERENCES

(1) Taylor, D. M.; Taylor, S. K. Environmental Uranium and Human Health. *Rev. Environ. Health* **1997**, *12* (3), 147.
(2) Jun, B.-M.; Kim, H.-H.; Rho, H.; Seo, J.; Jeon, J.-W.; Nam, S.-N.; Min Park, C.; Yoon, Y. Recovery of Rare-Earth and Radioactive Elements from Contaminated Water through Precipitation: A Review. *Chem. Eng. J.* **2023**, *475*, 146222.
(3) Smedley, P. L.; Kinniburgh, D. G. Uranium in Natural Waters and the Environment: Distribution, Speciation and Impact. *Appl. Geochem.* **2023**, *148*, 105534.
(4) Bailey, E. H.; Mosselmans, J. F. W.; Schofield, P. F. Uranyl Acetate Speciation in Aqueous Solutions—an XAS Study between 25°C and 250°C. *Geochim. Cosmochim. Acta* **2004**, *68* (8), 1711−1722.
(5) Kretzschmar, J.; Tsushima, S.; Lucks, C.; Jäckel, E.; Meyer, R.; Steudtner, R.; Müller, K.; Rossberg, A.; Schmeide, K.; Brendler, V. Dimeric and Trimeric Uranyl(VI)−Citrate Complexes in Aqueous Solution. *Inorg. Chem.* **2021**, *60* (11), 7998−8010.
(6) Yue, Y.-C.; Li, M.-H.; Wang, H.-B.; Zhang, B.-L.; He, W. The Toxicological Mechanisms and Detoxification of Depleted Uranium Exposure. *Environ. Health Prev. Med.* **2018**, *23* (1), 18.
(7) Becker, E. W.; Bier, K.; Bier, W.; Schütte, R.; Seidel, D. Separation of the Isotopes of Uranium by the Separation Nozzle Process. *Angew. Chem., Int. Ed. Engl.* **1967**, *6* (6), 507−518.
(8) Becker, E. W. Separation Nozzle. In *Uranium Enrichment*; Villani, S., Amelinckx, S., Gomer, R., Ibach, H., Lotsch, H. K. V., Schäfer, F. P., Ulrich, R., Wijn, H. P. J., Chebotayev, V. P., Hautojärvi, P., Letokhov, V. S., Queisser, H. J., Shimoda, K., Welford, W. T., Eds., Series Eds.; *Topics in Applied Physics*; Springer: Berlin Heidelberg: Berlin, Heidelberg, 1979; Vol. *35*, pp 245−268. DOI: .
(9) Campargue, R. Aerodynamic Separation Effect on Gas and Isotope Mixtures Induced by Invasion of the Free Jet Shock Wave Structure. *J. Chem. Phys.* **1970**, *52* (4), 1795−1802.
(10) Nikitenko, S. I. The Separation of Uranium Isotopes by Chemical Isotopic Exchange. *Russ. Chem. Rev.* **1989**, *58* (5), 441−452.
(11) Ikeda, A.; Hennig, C.; Tsushima, S.; Takao, K.; Ikeda, Y.; Scheinost, A. C.; Bernhard, G. Comparative Study of Uranyl(VI) and -(V) Carbonato Complexes in an Aqueous Solution. *Inorg. Chem.* **2007**, *46* (10), 4212−4219.
(12) Nocton, G.; Horeglad, P.; Vetere, V.; Pécaut, J.; Dubois, L.; Maldivi, P.; Edelstein, N. M.; Mazzanti, M. Synthesis, Structure, and Bonding of Stable Complexes of Pentavalent Uranyl. *J. Am. Chem. Soc.* **2010**, *132* (2), 495−508.
(13) Cumberland, S. A.; Douglas, G.; Grice, K.; Moreau, J. W. Uranium Mobility in Organic Matter-Rich Sediments: A Review of Geological and Geochemical Processes. *Earth-Sci. Rev.* **2016**, *159*, 160−185.
(14) O'Loughlin, E. J.; Kelly, S. D.; Cook, R. E.; Csencsits, R.; Kemner, K. M. Reduction of Uranium(VI) by Mixed Iron(II)/Iron(III) Hydroxide (Green Rust): Formation of UO_2 Nanoparticles. *Environ. Sci. Technol.* **2003**, *37* (4), 721−727.
(15) Liu, X.; Xie, Y.; Hao, M.; Li, Y.; Chen, Z.; Yang, H.; Waterhouse, G. I. N.; Wang, X.; Ma, S. Secondary Metal Ion-Induced Electrochemical Reduction of U(VI) to U(IV) Solids. *Nat. Commun.* **2024**, *15* (1), 7736.
(16) Căluşaru, A.; Bunuş, F. Separation of Uranium Isotopes by Ion Exchange: Part I. Behaviour of^{234} Th and^{234} Pa During the Uranium Band Displacement on Cation Exchange Resin by Acetate and Citrate Eluents. *Radiochim. Acta* **1972**, *18* (1), 23−30.
(17) Tanaka, Y.; Fujii, Y.; Okamoto, M. Raman Spectroscopic and Chromatographic Study of the Uranium Isotope Effect in Uranyl Acetate Complex Formation. *J. Phys. Chem.* **1982**, *86* (6), 1015−1018.
(18) Goda, R.; Sakuma, Y.; Fujii, Y.; Okamoto, M. Uranium Isotope Fractionation Occurred in Anion Exchange Chromatography Using Uranyl Acetate and Uranyl Citrate Complexes. *Isot. Isot. Environ. Health Stud.* **1982**, *18* (8), 293−295.
(19) Tanaka, Y.; Fukuda, J.; Okamoto, M.; Maeda, M. Infrared Spectroscopic and Chromatographic Studies on Uranium Isotope Effect in Formation of Uranyl Acetate, Citrate and Fluoride Complexes in Aqueous Solution. *J. Inorg. Nucl. Chem.* **1981**, *43* (12), 3291−3294.
(20) Choppin, G. R. Humics and Radionuclide Migration. *ract* **1988**, *44*−*45* (1), 23−28.
(21) Sachs, S.; Bernhard, G. Influence of Humic Acids on the Actinide Migration in the Environment: Suitable Humic Acid Model Substances and Their Application in Studies with Uranium—a Review. *J. Radioanal. Nucl. Chem.* **2011**, *290* (1), 17−29.
(22) *Isotope Effects In Chemistry and Biology*; Kohen, A., Limbach, H.-H., Eds.; CRC Press, 2005; ..
(23) Kim, H. Y.; Kakihana, M.; Aida, M.; Kogure, K.; Nomura, M.; Fujii, Y.; Okamoto, M. Uranium Isotope Effects in Some Ion Exchange Systems Involving Uranyl−Carboxylate Complexes. *J. Chem. Phys.* **1984**, *81* (12), 6266−6271.
(24) Aoyama, T.; Aida, M.; Fujii, Y.; Okamoto, M. Uranium Isotope Effects in Uranyl Carbonate Complex System. *J. Phys. Chem.* **1989**, *93* (6), 2666−2668.
(25) Sato, A.; Hada, M.; Abe, M. Electron Correlation Effects on Uranium Isotope Fractionation in U(vi)−U(vi) and U(iv)−U(vi) Equilibrium Isotopic Exchange Systems. *Phys. Chem. Chem. Phys.* **2024**, *26* (21), 15301−15315.
(26) Kakihana, M.; Nagumo, T.; Okamoto, M.; Kakihana, H. Coordination Structures for Uranyl Carboxylate Complexes in Aqueous Solution Studied by IR and Carbon-13 NMR Spectra. *J. Phys. Chem.* **1987**, *91* (24), 6128−6136.
(27) Du, X.; Boonchayaanant, B.; Wu, W.-M.; Fendorf, S.; Bargar, J.; Criddle, C. S. Reduction of Uranium(VI) by Soluble Iron(II)

Conforms with Thermodynamic Predictions. *Environ. Sci. Technol.* **2011**, *45* (11), 4718−4725.
(28) Di Bernardo, P.; Zanonato, P. L.; Benetollo, F.; Melchior, A.; Tolazzi, M.; Rao, L. Energetics and Structure of Uranium(VI)−Acetate Complexes in Dimethyl Sulfoxide. *Inorg. Chem.* **2012**, *51* (16), 9045−9055.
(29) Zhang, M.; Zhong, R.; Yu, C.; Cui, H. The Immobility of Uranium (U) in Metamorphic Fluids Explained by the Predominance of Aqueous U(IV). *Minerals* **2023**, *13* (3), 427.
(30) Tremaine, P. R.; Chen, J. D.; Wallace, G. J.; Boivin, W. A. Solubility of Uranium (IV) Oxide in Alkaline Aqueous Solutions to 300. C. *J. Solution Chem.* **1981**, *10* (3), 221−230.
(31) Clark, D. L.; Hobart, D. E.; Neu, M. P. Actinide Carbonte Complexes and Their Importance in Actinide Environmental Chemistry. *Chem. Rev.* **1995**, *95* (1), 25−48.
(32) Li, Y.; Su, J.; Mitchell, E.; Zhang, G.; Li, J. Photocatalysis with Visible-Light-Active Uranyl Complexes. *Sci. China Chem.* **2013**, *56* (12), 1671−1681.
(33) Lovley, D. R.; Phillips, E. J. P.; Gorby, Y. A.; Landa, E. R. Microbial Reduction of Uranium. *Nature* **1991**, *350* (6317), 413−416.
(34) Renshaw, J. C.; Butchins, L. J. C.; Livens, F. R.; May, I.; Charnock, J. M.; Lloyd, J. R. Bioreduction of Uranium: Environmental Implications of a Pentavalent Intermediate. *Environ. Sci. Technol.* **2005**, *39* (15), 5657−5660.
(35) Morris, D. E. Redox Energetics and Kinetics of Uranyl Coordination Complexes in Aqueous Solution. *Inorg. Chem.* **2002**, *41* (13), 3542−3547.
(36) Ilton, E. S.; Haiduc, A.; Cahill, C. L.; Felmy, A. R. Mica Surfaces Stabilize Pentavalent Uranium. *Inorg. Chem.* **2005**, *44* (9), 2986−2988.
(37) Ortu, F.; Randall, S.; Moulding, D. J.; Woodward, A. W.; Kerridge, A.; Meyer, K.; La Pierre, H. S.; Natrajan, L. S. Photoluminescence of Pentavalent Uranyl Amide Complexes. *J. Am. Chem. Soc.* **2021**, *143* (33), 13184−13194.
(38) Su, J.; Dau, P. D.; Qiu, Y.-H.; Liu, H.-T.; Xu, C.-F.; Huang, D.-L.; Wang, L.-S.; Li, J. Probing the Electronic Structure and Chemical Bonding in Tricoordinate Uranyl Complexes $UO_2X_3^-$ (X = F, Cl, Br, I): Competition between Coulomb Repulsion and U−X Bonding. *Inorg. Chem.* **2013**, *52* (11), 6617−6626.
(39) Denning, R. G. Electronic Structure and Bonding in Actinyl Ions and Their Analogs. *J. Phys. Chem. A* **2007**, *111* (20), 4125−4143.
(40) Su, J.; Wang, Y.-L.; Wei, F.; Schwarz, W. H. E.; Li, J. Theoretical Study of the Luminescent States and Electronic Spectra of UO_2Cl_2 in an Argon Matrix. *J. Chem. Theory Comput.* **2011**, *7* (10), 3293−3303.
(41) Su, J.; Zhang, K.; Schwarz, W. H. E.; Li, J. Uranyl-Glycine-Water Complexes in Solution: Comprehensive Computational Modeling of Coordination Geometries, Stabilization Energies, and Luminescence Properties. *Inorg. Chem.* **2011**, *50* (6), 2082−2093.
(42) Burns, C. J.; Neu, M. P.; Boukhalfa, H.; Gutowski, K. E.; Bridges, N. J.; Rogers, R. D. The Actinides. In *Comprehensive Coordination Chemistry II*; Elsevier, 2003; pp 189−345..
(43) Hu, S.-X.; Gibson, J. K.; Li, W.-L.; Van Stipdonk, M. J.; Martens, J.; Berden, G.; Redlich, B.; Oomens, J.; Li, J. Electronic Structure and Characterization of a Uranyl Di-15-Crown-5 Complex with an Unprecedented Sandwich Structure. *Chem. Commun.* **2016**, *52* (86), 12761−12764.
(44) Gong, Y.; Hu, H.-S.; Rao, L.; Li, J.; Gibson, J. K. Experimental and Theoretical Studies on the Fragmentation of Gas-Phase Uranyl−, Neptunyl−, and Plutonyl−Diglycolamide Complexes. *J. Phys. Chem. A* **2013**, *117* (40), 10544−10550.
(45) Hu, S.-X.; Jian, J.; Li, J.; Gibson, J. K. Destruction of the Uranyl Moiety in a U(V) "Cation−Cation" Interaction. *Inorg. Chem.* **2019**, *58* (15), 10148−10159.
(46) Fromager, E.; Vallet, V.; Schimmelpfennig, B.; Macak, P.; Privalov, T.; Wahlgren, U. Spin−Orbit Effects in Electron Transfer in Neptunyl(VI)−Neptunyl(V) Complexes in Solution. *J. Phys. Chem. A* **2005**, *109* (22), 4957−4960.
(47) Burdet, F.; Pécaut, J.; Mazzanti, M. Isolation of a Tetrameric Cation−Cation Complex of Pentavalent Uranyl. *J. Am. Chem. Soc.* **2006**, *128* (51), 16512−16513.
(48) *The Chemistry of the Actinide and Transactinide Elements*; Morss, L. R., Edelstein, N. M., Fuger, J., Eds.; Springer Netherlands: Dordrecht, 2011; ..
(49) Arnold, P. L.; Love, J. B.; Patel, D. Pentavalent Uranyl Complexes. *Coord. Chem. Rev.* **2009**, *253* (15−16), 1973−1978.
(50) Wood, S. A.; Van Middlesworth, J. The Influence of Acetate and Oxalate as Simple Organic Ligands on the Behavior of Palladium in Surface Environments. *Can. Mineral.* **2004**, *42* (2), 411−421.
(51) Groenewold, G. S.; De Jong, W. A.; Oomens, J.; Van Stipdonk, M. J. Variable Denticity in Carboxylate Binding to the Uranyl Coordination Complexes. *J. Am. Soc. Mass Spectrom.* **2010**, *21* (5), 719−727.
(52) De Jong, W. A.; Aprà, E.; Windus, T. L.; Nichols, J. A.; Harrison, R. J.; Gutowski, K. E.; Dixon, D. A. Complexation of the Carbonate, Nitrate, and Acetate Anions with the Uranyl Dication: Density Functional Studies with Relativistic Effective Core Potentials. *J. Phys. Chem. A* **2005**, *109* (50), 11568−11577.
(53) Schlosser, F.; Krüger, S.; Rösch, N. A Density Functional Study of Uranyl Monocarboxylates. *Inorg. Chem.* **2006**, *45* (4), 1480−1490.
(54) Perez, E.; Hanley, C.; Koehler, S.; Pestok, J.; Polonsky, N.; Van Stipdonk, M. Gas Phase Reactions of Ions Derived from Anionic Uranyl Formate and Uranyl Acetate Complexes. *J. Am. Soc. Mass Spectrom.* **2016**, *27* (12), 1989−1998.
(55) Dau, P. D.; Dau, P. V.; Rao, L.; Kovács, A.; Gibson, J. K. A Uranyl Peroxide Dimer in the Gas Phase. *Inorg. Chem.* **2017**, *56* (7), 4186−4196.
(56) Pereira, C. C. L.; Michelini, M. D. C.; Marçalo, J.; Gong, Y.; Gibson, J. K. Synthesis and Properties of Uranium Sulfide Cations. An Evaluation of the Stability of Thiouranyl, $\{S = U=S\}^{2+}$. *Inorg. Chem.* **2013**, *52* (24), 14162−14167.
(57) Gong, Y.; De Jong, W. A.; Gibson, J. K. Gas Phase Uranyl Activation: Formation of a Uranium Nitrosyl Complex from Uranyl Azide. *J. Am. Chem. Soc.* **2015**, *137* (18), 5911−5915.
(58) Gong, Y.; Gibson, J. K. Formation and Characterization of the Uranyl−SO_2 Complex, $UO_2(CH_3SO_2)(SO_2)^-$. *J. Phys. Chem. A* **2013**, *117* (4), 783−787.
(59) Steppert, M.; Walther, C.; Fuss, M.; Büchner, S. On the Polymerization of Hexavalent Uranium. An Electrospray Mass Spectrometry Study. *Rapid Commun. Mass Spectrom.* **2012**, *26* (6), 583−591.
(60) De Jong, W. A.; Dau, P. D.; Wilson, R. E.; Marçalo, J.; Van Stipdonk, M. J.; Corcovilos, T. A.; Berden, G.; Martens, J.; Oomens, J.; Gibson, J. K. Revealing Disparate Chemistries of Protactinium and Uranium. Synthesis of the Molecular Uranium Tetroxide Anion, UO_4^-. *Inorg. Chem.* **2017**, *56* (6), 3686−3694.
(61) Van Stipdonk, M. J.; Chien, W.; Anbalagan, V.; Bulleigh, K.; Hanna, D.; Groenewold, G. S. Gas-Phase Complexes Containing the Uranyl Ion and Acetone. *J. Phys. Chem. A* **2004**, *108* (47), 10448−10457.
(62) Marshall, M.; Zhu, Z.; Harris, R.; Collins, E.; Bowen, K. H. Photoelectron Spectroscopic Study of Ascorbate and Deprotonated Ascorbate Anions Using an Electrospray Ion Source and a Cryogenically Cooled Ion Trap. *J. Phys. Chem. A* **2021**, *125* (35), 7699−7704.
(63) Zhu, Z.; Marshall, M.; Harris, R.; Collins, E.; Bowen, K. H. Photoelectron Spectroscopic and Computational Study of the Deprotonated Gallic Acid and Propyl Gallate Anions. *J. Am. Soc. Mass Spectrom.* **2022**, *33* (8), 1355−1361.
(64) Vázquez, J.; Bo, C.; Poblet, J. M.; De Pablo, J.; Bruno, J. DFT Studies of Uranyl Acetate, Carbonate, and Malonate, Complexes in Solution. *Inorg. Chem.* **2003**, *42* (19), 6136−6141.
(65) Dunning, T. H., Jr. Gaussian Basis Sets for Use in Correlated Molecular Calculations. I. The Atoms Boron through Neon and Hydrogen. *J. Chem. Phys.* **1989**, *90* (2), 1007−1023.

https://doi.org/10.1021/acs.jpca.6c00067
J. Phys. Chem. A 2026, 130, 1829−1836

(66) Kendall, R. A.; Dunning, T. H.; Harrison, R. J. Electron Affinities of the First-Row Atoms Revisited. Systematic Basis Sets and Wave Functions. *J. Chem. Phys.* **1992**, *96* (9), 6796−6806.
(67) Peterson, K. A. Correlation Consistent Basis Sets for Actinides. I. The Th and U Atom. *J. Chem. Phys.* **2015**, *142* (7), 074105.
(68) Dolg, M.; Cao, X. Accurate Relativistic Small-Core Pseudopotentials for Actinides. Energy Adjustment for Uranium and First Applications to Uranium Hydride. *J. Phys. Chem. A* **2009**, *113* (45), 12573−12581.
(69) Frisch, M. J.; Trucks, G. W.; Schlegel, H. B.; Scuseria, G. E.; Robb, M. A.; Cheeseman, J. R.; Scalmani, G.; Barone, V.; Petersson, G. A.; Nakatsuji, H.; Li, X.; Caricato, M.; Marenich, A. V.; Bloino, J.; Janesko, B. G.; Gomperts, R.; Mennucci, B.; Hratchian, H. P.; Ortiz, J. V.; Izmaylov, A. F.; Sonnenberg, J. L.; Williams-Young, D.; Ding, F.; Lipparini, F.; Egidi, F.; Goings, J.; Peng, B.; Petrone, A.; Henderson, T.; Ranasinghe, D.; Zakrzewski, V. G.; Gao, J.; Rega, N.; Zheng, G.; Liang, W.; Hada, M.; Ehara, M.; Toyota, K.; Fukuda, R.; Hasegawa, J.; Ishida, M.; Nakajima, T.; Honda, Y.; Kitao, O.; Nakai, H.; Vreven, T.; Throssell, K.; Montgomery, J. A., Jr.; Peralta, J. E.; Ogliaro, F.; Bearpark, M. J.; Heyd, J. J.; Brothers, E. N.; Kudin, K. N.; Staroverov, V. N.; Keith, T. A.; Kobayashi, R.; Normand, J.; Raghavachari, K.; Rendell, A. P.; Burant, J. C.; Iyengar, S. S.; Tomasi, J.; Cossi, M.; Millam, J. M.; Klene, M.; Adamo, C.; Cammi, R.; Ochterski, J. W.; Martin, R. L.; Morokuma, K.; Farkas, O.; Foresman, J. B.; Fox, D. J. Gaussian 16, Revision C.01. Gaussian, Inc.: Wallingford CT, 2016.
(70) Werner, H.-J.; Knowles, P. J.; Celani, P.; Gyorffy, W.; Hesselmann, A.; Kats, D.; Knizia, G.; Kohn, A.; Korona, T.; Kreplin, D.; Lindh, R.; Ma, Q.; Manby, F. R.; Mitrushenkov, A.; Rauhut, G.; Schutz, M.; Shamasundar, K. R.; Adler, T. B.; Amos, R. D.; Baker, J.; Bennie, S. J.; Bernhardsson, A.; Berning, A.; Black, J. A.; Bygrave, P. J.; Cimiraglia, R.; Cooper, D. L.; Coughtrie, D.; Deegan, M. J. O.; Dobbyn, A. J.; Doll, K.; Dornbach, M.; Eckert, F.; Erfort, S.; Goll, E.; Hampel, C.; Hetzer, G.; Hill, J. G.; Hodges, M.; Hrenar, T.; Jansen, G.; Koppl, C.; Kollmar, C.; Lee, S. J. R.; Liu, Y.; Lloyd, A. W.; Mata, R. A.; May, A. J.; Mussard, B.; McNicholas, S. J.; Meyer, W.; Miller III, T. F.; Mura, M. E.; Nicklass, A.; O'Neill, D. P.; Palmieri, P.; Peng, D.; Peterson, K. A.; Pfluger, K.; Pitzer, R.; Polyak, I.; Pulay, P.; Reiher, M.; Richardson, J. O.; Robinson, J. B.; Schroder, B.; Schwilk, M.; Shiozaki, T.; Sibaev, M.; Stoll, H.; Stone, A. J.; Tarroni, R.; Thorsteinsson, T.; Toulouse, J.; Wang, M.; Welborn, M.; Ziegler, B. MOLPRO, version 2021.3, a package of ab initio programs. See https://www.molpro.net.
(71) Haynes, W. M.; Lide, D. R.; Bruno, T. J. *CRC Handbook of Chemistry and Physics: A Ready Reference Book of Chemical and Physical Data*, 93rd ed.; CRC: Boca Raton, 2012.
(72) Wang, X.-B.; Woo, H.-K.; Wang, L.-S.; Minofar, B.; Jungwirth, P. Determination of the Electron Affinity of the Acetyloxyl Radical (CH_3 COO) by Low-Temperature Anion Photoelectron Spectroscopy and Ab Initio Calculations. *J. Phys. Chem. A* **2006**, *110* (15), 5047−5050.
(73) Dekock, R. L.; Baerends, E. J.; Boerrigter, P. M.; Snijders, J. G. On the Nature of the First Excited States of the Uranyl Ion. *Chem. Phys. Lett.* **1984**, *105* (3), 308−316.
(74) Pierloot, K.; Van Besien, E. Electronic Structure and Spectrum of UO22+ and UO2Cl42. *J. Chem. Phys.* **2005**, *123* (20), 204309.
(75) Merritt, J. M.; Han, J.; Heaven, M. C. Spectroscopy of the UO2+ Cation and the Delayed Ionization of UO2. *J. Chem. Phys.* **2008**, *128* (8), 084304.
(76) Kovács, A.; Konings, R. J. M.; Gibson, J. K.; Infante, I.; Gagliardi, L. Quantum Chemical Calculations and Experimental Investigations of Molecular Actinide Oxides. *Chem. Rev.* **2015**, *115* (4), 1725−1759.
(77) Ghosh, R.; Mondal, J. A.; Ghosh, H. N.; Palit, D. K. Ultrafast Dynamics of the Excited States of the Uranyl Ion in Solutions. *J. Phys. Chem. A* **2010**, *114* (16), 5263−5270.
(78) Kozimor, S. A.; Yang, P.; Batista, E. R.; Boland, K. S.; Burns, C. J.; Clark, D. L.; Conradson, S. D.; Martin, R. L.; Wilkerson, M. P.; Wolfsberg, L. E. Trends in Covalency for D- and f-Element Metallocene Dichlorides Identified Using Chlorine K-Edge X-Ray Absorption Spectroscopy and Time-Dependent Density Functional Theory. *J. Am. Chem. Soc.* **2009**, *131* (34), 12125−12136.

https://doi.org/10.1021/acs.jpca.6c00067
J. Phys. Chem. A 2026, 130, 1829−1836